 doi:10.20944/preprints202010.0619.v1

Article

Crystallization of optically thick amorphous silicon films by near-IR femtosecond laser processing

Kirill Bronnikov [1,2], Alexander Dostovalov [1,2], Artem Cherepakhin[3], Eugeny Mitsai [3], Alexander Nepomniaschiy [3], Sergei A. Kulinich[4,5], Alexey Zhizhchenko [3,4] and Aleksandr Kuchmizhak [3,4]*

1 Institute of Automation and Electrometry of the SB RAS, 1 Acad. Koptyug Ave., Novosibirsk 630090, Russia
2 Novosibirsk State University, 2 Pirogova St., Novosibirsk 630090, Russia
3 Institute of Automation and Control Processes FEB RAS, 5 Radio St., Vladivostok 690041, Russia
4 Far Eastern Federal University, Vladivostok 690041, Russia;
5 Research Institute of Science and Technology, Tokai University, Hiratsuka, Kanagawa 259-1292, Japan;
* Correspondence: alex.iacp.dvo@mail.ru; +7-914-070-1626 (A.K.)

Abstract: Amorphous silicon (α-Si) film present an inexpensive and promising material for optoelectronic and nanophotonic applications. Its basic optical and optoelectronic properties are known to be improved via phase transition from amorphous to polycrystalline phase. Infrared femtosecond laser radiation can be considered as a promising nondestructive and facile way to drive uniform in-depth and lateral crystallization of α-Si films that are typically opaque in UV-visible spectral range. However, so far only a few studies reported on utilization of near-IR radiation for laser-induced crystallization of α-Si providing no information regarding optical properties of the resultant polycrystalline Si films. The present work demonstrates efficient and gentle single-pass crystallization of α-Si films induced by their direct irradiation with near-IR femtosecond laser pulses coming at sub-MHz repetition rate. Comprehensive analysis of morphology and composition of laser-annealed films by atomic-force microscopy, optical, micro-Raman and energy-dispersive X-ray spectroscopy, as well as numerical modeling of optical spectra, confirmed efficient crystallization of α-Si and high-quality of the obtained films. Moreover, we highlight localized laser-driven crystallization of α-Si as a promising way for optical information encryption, anti-counterfeiting and fabrication of micro-optical elements.

Keywords: amorphous silicon; polycrystalline silicon; thin films; laser-induced annealing; femtosecond laser pulses; Raman spectroscopy

1. Introduction

Due to the advantages of polycrystalline silicon (poly-Si) over its amorphous counterpart (α-Si), which include orders of magnitude higher carrier mobility and better stability, thin films of poly-Si have become the basis for solar cells, thin-film transistors, high definition displays, vertically integrated memory devices, etc. [1–5]. Large scale poly-Si is traditionally obtained in a chemical reaction of hydrogen reduction of trichlorosilane $SiHCl_3$ in rod-type reactors (so-called "Siemens process") or by pyrolytic decomposition of monosilane SiH_4 in rod-type and boiling-layer-type reactors [6]. However, these methods include high-temperature exposure (700-1000 °C), thus restricting the choice of substrates to refractory materials and, therefore, cannot be used to produce low-temperature polycrystalline silicon (LTPS) which is currently the most promising material for polymer-based flexible displays requiring high-speed operation and high resolution [4]. Crystallization of amorphous silicon is an actively studied approach for obtaining poly-Si thin films since thin films of α-Si can be produced by cheap low-temperature chemical or physical vapor deposition over large-scale substrates

Preprints (www.preprints.org) | NOT PEER-REVIEWED | Posted: 29 October 2020 doi:10.20944/preprints202010.0619.v1

including glasses and flexible polymers, that allows to extend functionality and reduced fabrication cost of resulting optoelectronic devices. To improve optical properties and inherently low carrier mobility of α-Si films, multiple efforts were undertaken to perform conversion of amorphous Si material to its polycrystalline phase. More specifically, crystallization of α-Si was realized using thermal annealing [7], solid-phase crystallization[8], metal-induced crystallization and modifications of this method for lateral crystallization [9,10]. All these methods are usually accompanied by a melting-cooling-solidification cycle.

In recent decades, laser annealing was recognized as a flexible technique to locally crystallize α-Si with high control [11]. In particular, the use of excimer laser with ultraviolet (UV) radiation was previously justified to efficiently drive transition of amorphous Si to its polycrystalline phase allowing to produce high-quality films [12–15]. However, ultra-low penetration depth of UV light to silicon limits the thickness of α-Si film, which can be processed with such an approach. Visible laser radiation (in particular, blue and green lasers operating in CW and pulsed mode [1,16–20]) was shown to increase the maximal processing thickness to 150-200 nm; however, this is still not enough to cover all applications. Noteworthy, penetration depth of near-IR radiation into Si, which has good transparency in this spectral range (comparing to UV and visible light), is high enough to drive crystallization inside rather thick α-Si films that are required for realistic applications and devices. On the other hand, CW or down to nanosecond pulsed regimes need relatively high fluence levels to initiate the melting and do not offer precise spatial material processing [21,22].

Femtosecond radiation opens up new possibilities in laser-induced crystallization exploiting nonlinear pulses energy absorption that results in high spatial localization of material modification and low fluence threshold for crystallization in comparison with longer pulses due to minimization of heat diffusion [23,24]. It was previously found that the fluence threshold depends on the laser wavelength, being lower when using the second harmonics (λ = 400 nm), which was explained by a shallower melting depth in the case of shorter wavelengths [25]. It was also shown that, in comparison with other experimental parameters (pulse duration, polarization, number of pulses, etc.), the substrate temperature significantly affects the crystallization process reducing the threshold down from 65 mJ/cm^2 to 49 mJ/cm^2 when increasing the temperature from 25 to 200 °C [26]. Various dependencies of the poly-Si characteristics on the laser processing parameters were reported recently: the size of the crystallites [27], crystallization area homogeneity [28], photoelectric properties [29], and surface morphology [30]. However, so far only a few studies reported utilization of near-IR radiation for laser-induced crystallization of α-Si films providing information regarding optical properties of the annealed poly-Si films [26,31–33].

Here, we used near-IR femtosecond laser pulses to directly drive phase transition of glass-supported 365-nm thick α-Si, which resulted in formation of high-quality poly-Si passivated with nanometer-thick silicon dioxide overlayer. Elliptically-shaped laser beam with an aspect ratio of 10 was used to improve the uniformity of laser-annealed areas. Composition and crystallinity of obtained films were verified with Raman and energy-dispersive X-ray spectroscopy, while comparative atomic-force microscopic (AFM) analysis of the produced poly-Si and as-deposited α-Si samples revealed a very small increase of surface roughness from 0.5 to 1.3 nm upon laser texturing. Optical spectroscopic studies supported by numerical modeling confirmed improved optical characteristics of laser-annealed films in the visible spectral range associated with reduction of the absorption coefficient associated with polycrystalline phase.

2. Materials and methods

α-Si films with a thickness of 365±5 nm were deposited onto a borosilicate glass plate by magnetron sputtering and used for laser annealing without any pre-treatment. Direct laser-induced crystallization of such films was performed using femtosecond (pulse duration of 230 fs) IR (wavelength of 1026 nm) laser pulses generated by a regeneratively-amplified Yb:KGW laser system (Pharos, Light Conversion Ltd., Vilnius, Lithuania) at a maximal pulse repetition rate of 200 KHz.

Preprints (www.preprints.org) | NOT PEER-REVIEWED | Posted: 29 October 2020 doi:10.20944/preprints202010.0619.v1

The Gaussian-shaped beam generated by the laser system was passing through a cylindrical concave lens with the focal distance of -1 m and then was focused by a convex lens with the focal distance of 50 mm (Fig. 1a). The resulting intensity distribution in the focal plane presented elliptically shaped beam with a size of 160 μm along long axis and the axes ratio of 1:10. Based on our previous studies [34], pulse energy and scanning speed were chosen to be 1.5 μJ and 1 mm/s, respectively. The samples were arranged onto a 2D motorized platform (Aerotech Gmbh., Nurnberg, Germany) permitting to pattern rather large surface areas by merging with a certain overlap line scans produced with the elliptical-shaped laser beam. Localized laser-annealing was performed by focusing the IR laser radiation with a dry microscope lens with a numerical aperture of 0.8 that yielded in 1/e-diameter of the laser spot in the focal plane $\approx$ 1 μm. Same fluence and scanning speed were used to record microscale.

Laser-annealed areas of the α-Si film were carefully characterized by scanning electron microscopy (SEM, Ultra 55+, Carl Zeiss, Oberkochen, Germany) equipped with an energy-dispersive X-ray detector (EDX; X-max, Oxford Instruments, Abingdon, United Kingdom), as well as atomic-force microscopy (AFM, Nano-DST, Pacific Nanotechnology, USA). Transmission and reflection spectra in the ultraviolet (UV) and visible spectral range (200-1600 nm) were acquired using optical integrating sphere spectrometer (Cary 5000, Agilent Technologies, Santa Clara, USA). Raman measurements were undertaken with 532-nm wavelength CW laser fiber-coupled to micro-Raman microscope (Alpha 300, WiTec GmbH, Ulm, Germany). Each representative single spectrum was averaged over 50 times at different sample sites, while the signal integration time was 180 s. In the mapping regime, the signal integration time in each spot was 1 s. Pump laser intensity was chosen to avoid any possible laser-induced modification of α-Si even after several minutes of exposure.

3. Results and discussions

Laser irradiation of sample surfaces was performed at fixed pulse energy of 1.5 μJ and sample scanning speed V of 1 mm/s. At maximal available pulse repetition rate, such processing parameters ensured gentle laser-induced modification (crystallization) of the material without formation of so-called laser-induced periodic surface structures induced by corresponding in-plane modulation of the laser intensity [35–37]. Such a modulation oriented along the polarization vector was justified to originate from interference of the incident and scattered laser radiation. The surface morphology modification (typically oxidation, [34]) is known to start at interference maxima where laser intensity reaches the corresponding threshold fluence. It should be noted that faster scanning speed at such a fluence provided no visible laser-induced modification, indicating threshold behavior of the process.

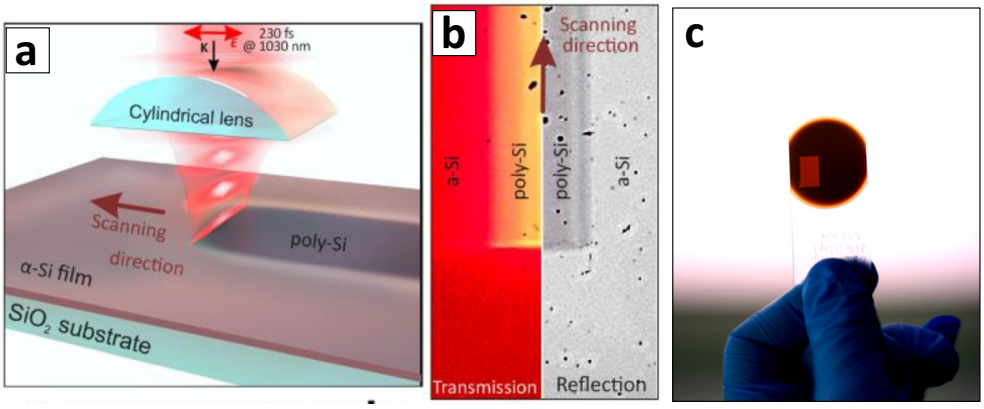

Figure 1. (**a**) Scheme of laser-induced annealing of α-Si films. (**b**) Reflection and transmission optical microscope images of produced poly-Si stripe surrounded by pristine α-Si film. (**c**) Optical image of uniform 1 cm^2 poly-Si area recorded in α-Si film.

Preprints (www.preprints.org) | NOT PEER-REVIEWED | Posted: 29 October 2020 doi:10.20944/preprints202010.0619.v1

Laser-modified α-Si film areas processed at optimal parameters demonstrate changed optical properties, which can be seen in optical reflection and transmission images (Fig. 1b). In particular, the yellowish color in the transmission optical image indicates corresponding modification of the transmission properties of the laser-treated area with respect to those of pristine sample. Optical photography (Fig. 1c) of the glass-supported α-Si film also illustrates higher transmission within a rather large ($\approx$ 1 cm^2) rectangular-shaped laser-processed area that was produced at optimal parameters by merging line scans at a step of 30 μm.

Importantly, SEM inspection of the laser-modified α-Si surface indicated no significant changes of surface morphology that could be observed. Comparative AFM analysis revealed a very small increase in surface roughness (Ra) from 0.5 to 1.3 nm upon laser texturing of pristine α-Si film (Fig. 2a). Such roughening can be partially attributed to a certain amount of nanoparticles that can be generated and deposited from the surface areas processed during dose tests. EDX analysis of the chemical composition performed at an accelerating voltage of 20 kV revealed a certain increase in oxygen fraction from 12 to 23 % in the laser-processed area potentially indicating formation of a nanometer-thick oxidized layer (Fig. 2b).

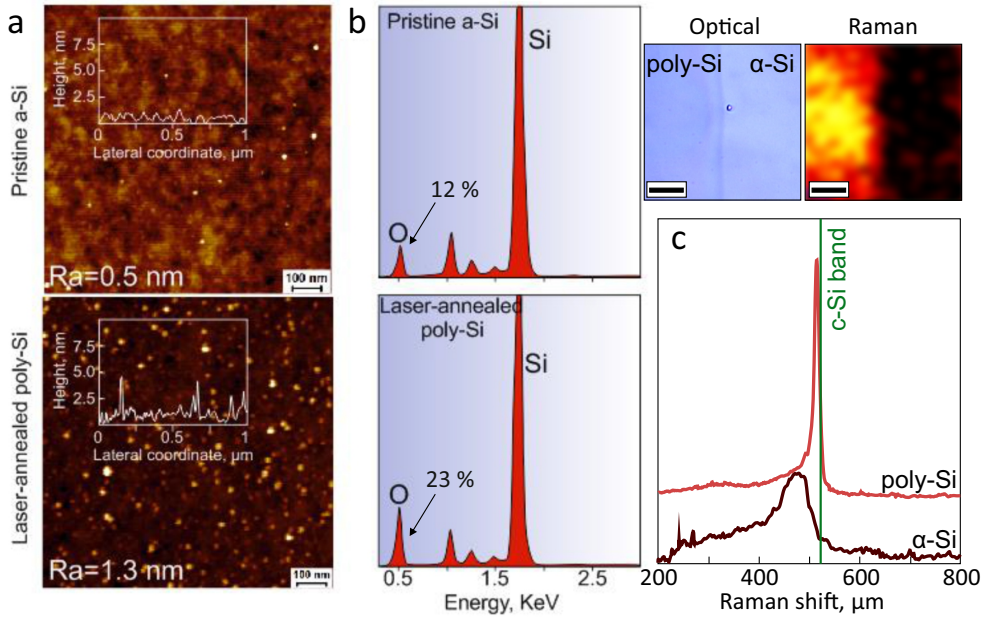

Figure 2. (**a**) AFM images revealing surface morphology and roughness of pristine α-Si and laser-annealed poly-Si films. (**b,c**) EDX and Raman spectra of pristine α-Si and laser-annealed poly-Si. Insets in **(c)** provide correlated contrasted optical and micro-Raman (@518$\pm$3 cm^{-1}) images taken near the boundary between pristine and annealed poly-Si. Scale bar in both images indicates 7 μm.

Raman microspectroscopy was used to further probe crystallinity of the laser-annealed areas. Representative averaged Raman spectra of pristine α-Si and laser-fabricated poly-Si are shown in Fig. 2c. If compared with untreated α-Si film that only demonstrated a low-intensity broad Raman band centered at 480 cm^{-1}, the laser-annealed poly-Si shows a sharp peak at 518 cm^{-1} which is slightly shifted with respect to the reference Raman frequency of monocrystalline Si at 520.8 cm^{-1} (shown by a vertical line in Fig. 2c). This spectral shift is indicative of nanocrystalline Si phase [38]. Mapping the intensity of this Raman band (518$\pm$4 cm^{-1}) near the boundary between pristine and laser-annealed areas allowed us easily to separate poly-Si and α-Si phase areas (see top insets in Fig. 2c).

Further, to reveal the difference in optical constants (refractive index, n, and absorption coefficient, k) between the pristine and laser-annealed films, we measured their UV-vis-IR reflection/transmission spectra. For both samples, their transmission/reflection coefficients were found to demonstrate typical Fabry-Perot modulations. However, for the laser-annealed poly-Si the modulation amplitude increases

Preprints (www.preprints.org) | NOT PEER-REVIEWED | Posted: 29 October 2020 doi:10.20944/preprints202010.0619.v1

(especially in the visible spectral range), indicating a certain decrease of k. Moreover, a distinct blueshift of the reflection/transmission spectra observed for the poly-Si film (with respect to those of the pristine α-Si) indicates corresponding change of the n value.

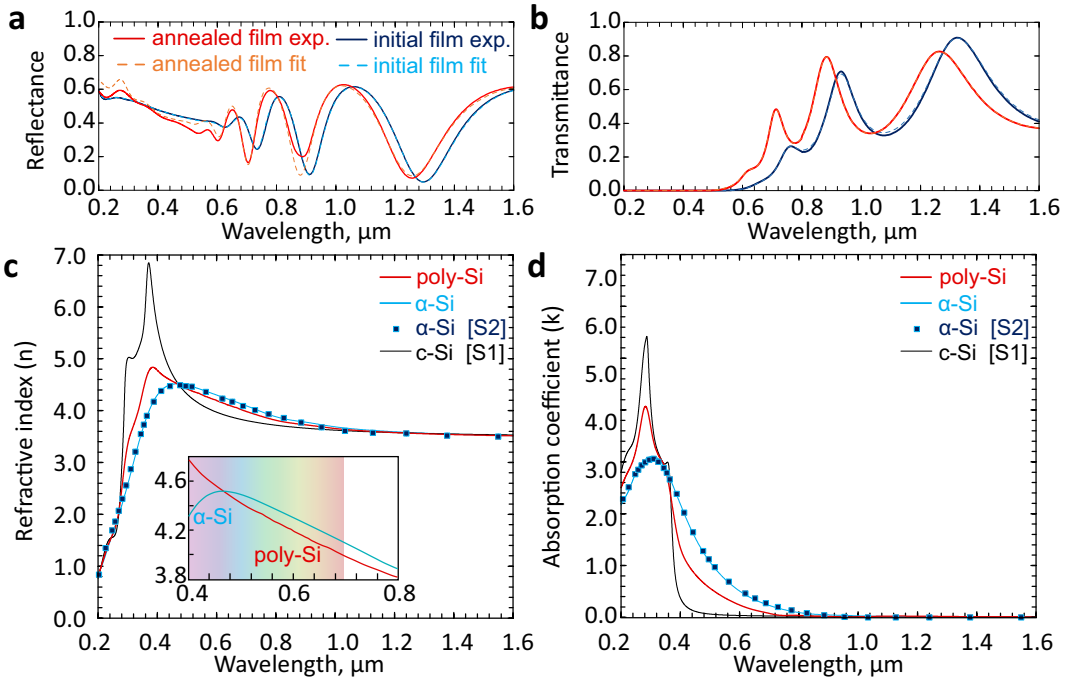

Figure 3. (**a,b**) Measured and calculated reflection and transmission spectra of pristine α-Si and laser-annealed poly-Si films. Solid curves provide experimental data while dashed curves present numerical fit. (**c,d**) Refractive index (n) and absorption coefficient (k) of pristine α-Si (blue solid curve) and laser-annealed (red solid curve) poly-Si film calculated from experimentally measured optical spectra. Inset in (c) highlights difference in refractive index of pristine and laser-annealed films in the visible spectral range. Markers in (c,d) give reference data for amorphous Si (α-Si, [39]) and monocrystalline Si (c-Si, black curve, [40]).

Based on the obtained reflection/transmission spectra, both the refractive index n and absorption coefficient k were further evaluated using common photometric approach [41,42] (see also Methods for details). The results of these calculations are summarized in Fig. 3(c,d) along with the reference data for amorphous [39] and monocrystalline bulk silicon [40]. Noteworthy, the obtained dispersion curves for pristine α-Si film perfectly fit the corresponding reference data [39], indicating correctness of the measurements and calculations. Also, transmission spectra obtained with such a numerical fit demonstrate excellent agreement with the experimental data (see dashed curves in Fig. 3a). As seen in Fig.3, for the laser-annealed poly-Si film the absorption coefficient decreases twice in the visible spectral range. Its obtained refractive index also decreases with respect to that of the pristine film by about 0.1 refractive index units (RIU) in the visible spectral range (at wavelength >500 nm) and increases largely in the blue part of the spectrum, following the trend similar to dispersion curve for monocrystalline Si. These features are indicative for polycrystalline silicon and are generally consistent with the previously reported studies for laser-annealed films [43]. Finally, the gentle fs-laser annealing applied is seen to cause a minimal effect on the morphology of silicon films as confirmed by SEM/AFM measurements. In combination with a significant laser-induced changes of refractive index ($\approx$ 0.1 RIU; see inset in Fig. 3c) and a considerable increase of transmission coefficient (decrease of k) in the yellow-red spectral range, this feature makes direct fs-laser processing of inexpensive α-Si films promising for optical information storage, anti-counterfeiting and recording of various planar micro-optical elements (for example, waveguides, Fresnel lenses and diffraction gratings). However,

Preprints (www.preprints.org) | NOT PEER-REVIEWED | Posted: 29 October 2020 doi:10.20944/preprints202010.0619.v1

at this point, demonstration of such elements and their performance is out of scope of this paper and will be a subject of our forthcoming studies.

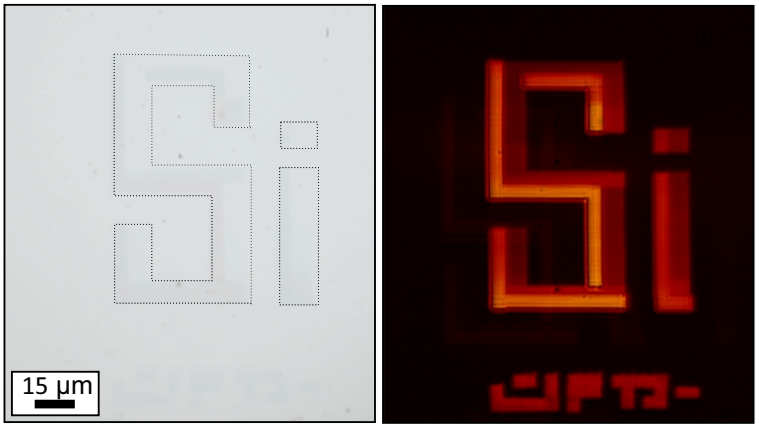

Figure 4. Reflection (left) and transmission (right) optical images of α-Si film containing laser-annealed microscale c-Si areas arranged to form "Si" letters. Black dashed lines highlight the location of laser-annealed area in the reflection image.

Nevertheless, in the end of this report, we demonstrate how fs-laser radiation can drive local crystallization of α-Si at the microscale, opening pathways for the above mentioned applications. We took advantage of a considerable decrease of k for poly-Si to encrypt "Si" letters in the pristine film via localized laser annealing (Fig. 4). These letters can hardly be resolved in the reflection-mode optical image appearing only under their visualization in transmission regime.

4. Conclusions

In conclusion, this work demonstrates that near-IR femtosecond laser pulses can efficiently drive phase transition in glass-supported 365-nm thick α-Si, resulting in formation of high-quality uniform polycrystalline Si passivated with a SiO_2 nanolayer. Composition and crystallinity of the obtained poly-Si film was verified with Raman and energy-dispersive X-ray spectroscopy, while comparative atomic-force microscopy analysis of the as-deposited α-Si and produced poly-Si films revealed very small increase of surface roughness from 0.5 to 1.3 nm upon laser texturing. Optical spectroscopy supported by numerical modeling confirmed improved optical characteristics of the laser-annealed poly-Si films in the visible and near-IR spectral range, which is associated with lower losses in the poly-Si phase. Direct femtosecond processing can be optimized to uniformly anneal α-Si over large-scale surface area or drive phase transition in a local volume. In particular, tight focusing of fs-laser radiation with high-NA optics is expected to provide a lateral resolution that is close to radiation wavelength (1030 nm in our experiments), thus opening pathways for fabrication of IR micro-optics and optical information encryption at 25,000 dpi. Chemical etching combined with laser processing can further enrich potential designs. Moreover, laser beam shaping with diffraction optical elements or spatial light modulators will apparently permit to optimize laser annealing process via proper laser energy delivery into α-Si material [44].

Author Contributions: conceptualization, A.A.K. and A.D.; methodology, A.D.,K.B.,E.M. and A.N.; software, A.Z.; validation, A.Z. and A.A.K.; formal analysis, A.A.K. and A.Z.; investigation, E.M. and K.B.; resources, A.A.K.; data curation, A.A.K.; writing–original draft preparation, A.D., A.Z. and A.A.K; writing–review and editing, A.A.K. and S.A.K.; visualization, A.Z. and A.A.K.; supervision, A.A.K.; project administration, A.A.K.; funding acquisition, A.D. and A.A.K.

Funding: This work was supported by Russian Foundation for Basic Research (projects nos. 20-32-70056, 19-32-90235).

Acknowledgments:

Conflicts of Interest: The authors declare no conflict of interest.

References

1. Jin, S.; Choe, Y.; Lee, S.; Kim, T.W.; Mativenga, M.; Jang, J. Lateral grain growth of amorphous silicon films with wide thickness range by blue laser annealing and application to high performance poly-Si TFTs. *IEEE Electron Device Letters* **2016**, *37*, 291–294.
2. Schropp, R.E.; Carius, R.; Beaucarne, G. Amorphous silicon, microcrystalline silicon, and thin-film polycrystalline silicon solar cells. *MRS bulletin* **2007**, *32*, 219–224.
3. Kamins, T. *Polycrystalline silicon for integrated circuit applications*; Vol. 45, Springer Science & Business Media, 2012.
4. Fortunato, G.; Pecora, A.; Maiolo, L. Polysilicon thin-film transistors on polymer substrates. *Materials Science in Semiconductor Processing* **2012**, *15*, 627–641.
5. Nickel, N.H. *Laser Crystallization of Silicon-Fundamentals to Devices*; Academic Press, 2003.
6. Yang, D. *Handbook of Photovoltaic Silicon*; Springer, 2019.
7. Wan, Z.; Huang, S.; Green, M.A.; Conibeer, G. Rapid thermal annealing and crystallization mechanisms study of silicon nanocrystal in silicon carbide matrix. *Nanoscale research letters* **2011**, *6*, 129.
8. Anderson, R. Microstructural analysis of evaporated and pyrolytic silicon thin films. *Journal of The Electrochemical Society* **1973**, *120*, 1540.
9. Hultman, L.; Robertsson, A.; Hentzell, H.; Engström, I.; Psaras, P. Crystallization of amorphous silicon during thin-film gold reaction. *Journal of applied physics* **1987**, *62*, 3647–3655.
10. Yuen, C.; Poon, M.; Chan, W.; Qin, M. Investigation of grain formation and growth in nickel-induced lateral crystallization process. *Journal of applied physics* **2002**, *92*, 6291–6295.
11. Andrä, G.; Bergmann, J.; Falk, F.; Ose, E.; Stafast, H. Laser induced crystallization of amorphous silicon films on glass for thin film solar cells. *Physica status solidi (a)* **1998**, *166*, 629–634.
12. Sameshima, T.; Hara, M.; Usui, S. XeCl excimer laser annealing used to fabricate poly-Si TFT's. *Jpn. J. Appl. Phys.* **1989**, *28*, 1789.
13. Smith, P.; Carey, P.; Sigmon, T. Excimer laser crystallization and doping of silicon films on plastic substrates. *Appl. Phys. Lett.* **1997**, *70*, 342–344.
14. Miyasaka, M.; Stoemenos, J. Excimer laser annealing of amorphous and solid-phase-crystallized silicon films. *J. Appl. Phys.* **1999**, *86*, 5556–5565.
15. Shih, A.; Meng, C.; Lee, S.; Chern, M. Mechanism for pillar-shaped surface morphology of polysilicon prepared by excimer laser annealing. *J. Appl. Phys.* **2000**, *88*, 3725–3733.
16. Do, Y.; Jeong, D.; Lee, S.; Kang, S.; Jang, S.; Jang, J. Remarkable Improvement in Foldability of Poly-Si Thin-Film Transistor on Polyimide Substrate Using Blue Laser Crystallization of Amorphous Si and Comparison with Conventional Poly-Si Thin-Film Transistor Used for Foldable Displays. *J. Appl. Phys.* **2020**, *22*, 1901430.
17. Park, M.; Vangelatos, Z.; Rho, Y.; Park, H.; Jang, J.; Grigoropoulos, C. Remarkable Improvement in Foldability of Poly-Si Thin-Film Transistor on Polyimide Substrate Using Blue Laser Crystallization of Amorphous Si and Comparison with Conventional Poly-Si Thin-Film Transistor Used for Foldable Displays. *Thin Solid Films* **2020**, *696*, 137779.
18. Chou, C.; Lee, I.; Yang, P.; Hu, M.; Wang, C.; Wu, C.; Chien, Y.; Wang, K.; Cheng, H. Effects of crystallization mechanism on the electrical characteristics of green continuous-wave-laser-crystallized polycrystalline silicon thin film transistors. *Appl. Phys. Lett.* **2013**, *103*, 053515.
19. Xu, L.; Grigoropoulos, C.; King, T. High-performance thin-silicon-film transistors fabricated by double laser crystallization. *J. Appl. Phys.* **2006**, *99*, 034508.
20. Ashitomi, T.; Harada, T.; Okada, T.; Noguchi, T.; Nishikata, O.; Ota, A. Appearance of the p-channel performance of poly-Si TFTs with a metal S/D electrode using BLDA aiming for low-cost CMOS. *J. Inf. Disp.* **2017**, *18*, 185–189.
21. Hatano, M.; Moon, S.; Lee, M.; Suzuki, K.; Grigoropoulos, C.P. Excimer laser-induced temperature field in melting and resolidification of silicon thin films. *Journal of Applied Physics* **1999**, *87*, 36–43.
22. Dassow, R.; Köhler, J.R.; Helen, Y.; Mourgues, K.; Bonnaud, O.; Mohammed-Brahim, T.; Werner, J.H. Laser crystallization of silicon for high-performance thin-film transistors. *Semicond. Sci. Technol.* **2000**, *15*, L31–L34.

23. Choi, T.Y.; Hwang, D.J.; Grigoropoulos, C.P. Ultrafast laser-induced crystallization of amorphous silicon films. *Optical engineering* **2003**, *42*, 3383–3389.
24. Shieh, J.M.; Chen, Z.H.; Dai, B.T.; Wang, Y.C.; Zaitsev, A.; Pan, C.L. Near-infrared femtosecond laser-induced crystallization of amorphous silicon. *Appl. Phys. Lett.* **2004**, *85*, 1232–1234.
25. Izawa, Y.; Tokita, S.; Fujita, M.; Norimatsu, T.; Izawa, Y. Ultra fast melting process in femtosecond laser crystallization of thin a-Si layer. *Applied Surface Science* **2009**, *255*, 9764–9769.
26. Zhan, X.; Hou, M.; Ma, F.; Su, Y.; Chen, J.; Xu, H. Room temperature crystallization of amorphous silicon film by ultrashort femtosecond laser pulses. *Opt. Laser Technol.* **2019**, *112*, 363–367.
27. Pan, C.L.; Chen, K.W.; Wang, Y.C.; Kao, S.H.; Wu, P. Room-temperature crystallization of amorphous silicon by near-UV femtosecond pulses. *AIP Advances* **2020**, *10*, 055321.
28. Li, D.; Ilyas, N.; Song, Y.; Zhong, H.; Li, W.; Jiang, Y. Inhomogeneous crystallization of a-Si thin films irradiated by femtosecond laser. *Journal of Raman Spectroscopy* **2019**, *50*, 793–801.
29. Emelyanov, A.V.; Khenkin, M.V.; Kazanskii, A.G.; Forsh, P.A.; Kashkarov, P.K.; Gecevicius, M.; Beresna, M.; Kazansky, P.G. Femtosecond laser induced crystallization of hydrogenated amorphous silicon for photovoltaic applications. *Thin Solid Films* **2014**, *556*, 410–413.
30. Wang, H.; Kongsuwan, P.; Satoh, G.; Yao, Y.L. Femtosecond laser-induced simultaneous surface texturing and crystallization of a-Si:H thin film: morphology study. *Int J Adv Manuf Technol* **2013**, *65*, 1691–1703.
31. Wang, X.C.; Zheng, H.Y.; Tan, C.W.; Wang, F.; Yu, H.Y.; Pey, K.L. Femtosecond laser induced surface nanostructuring and simultaneous crystallization of amorphous thin silicon film. *Opt. Express, OE* **2010**, *18*, 19379–19385.
32. Nayak, B.; Gupta, M. Femtosecond-laser-induced-crystallization and simultaneous formation of light trapping microstructures in thin a-Si:H films. *Appl. Phys. A* **2007**, *89*, 663–667.
33. Nayak, B.; Eaton, B.; Selvan, J.; Mcleskey, J.; Gupta, M.; Romero, R.; Ganguly, G. Semiconductor laser crystallization of a-Si:H on conducting tin-oxide-coated glass for solar cell and display applications. *Appl. Phys. A* **2005**, *80*, 1077–1080.
34. Dostovalov, A.; Bronnikov, K.; Korolkov, V.; Babin, S.; Mitsai, E.; Mironenko, A.; Tutov, M.; Zhang, D.; Sugioka, K.; Maksimovic, J.; others. Hierarchical anti-reflective laser-induced periodic surface structures (LIPSS) on amorphous Si films for sensing applications. *Nanoscale* **2020**.
35. Öktem, B.; Pavlov, I.; Ilday, S.; Kalaycıoğlu, H.; Rybak, A.; Yavaş, S.; Erdoğan, M.; Ilday, F.Ö. Nonlinear laser lithography for indefinitely large-area nanostructuring with femtosecond pulses. *Nature photonics* **2013**, *7*, 897.
36. Makarov, S.; Tsypkin, A.; Voytova, T.; Milichko, V.; Mukhin, I.; Yulin, A.; Putilin, S.; Baranov, M.; Krasnok, A.; Morozov, I.; others. Self-adjusted all-dielectric metasurfaces for deep ultraviolet femtosecond pulse generation. *Nanoscale* **2016**, *8*, 17809–17814.
37. Shuleiko, D.; Potemkin, F.; Romanov, I.; Parhomenko, I.; Pavlikov, A.; Presnov, D.; Zabotnov, S.; Kazanskii, A.; Kashkarov, P. Femtosecond laser pulse modification of amorphous silicon films: control of surface anisotropy. *Laser Physics Letters* **2018**, *15*, 056001.
38. Yang, C.; Li, S. Size-dependent Raman red shifts of semiconductor nanocrystals. *The Journal of Physical Chemistry B* **2008**, *112*, 14193–14197.
39. Pierce, D.; Spicer, W. Electronic structure of amorphous Si from photoemission and optical studies. *Phys. Rev. B* **1972**, *5*, 3017.
40. Green, M. Self-consistent optical parameters of intrinsic silicon at 300 K including temperature coefficients. *Sol. Energy Mater. Sol. Cells* **2008**, *92*, 1305–1310.
41. Manifacier, J.; Gasiot, J.; Fillard, J. A simple method for the determination of the optical constants n, k and the thickness of a weakly absorbing thin film. *J. Phys. E* **1976**, *9*, 1002.
42. Jin, Y.; Song, B.; Jia, Z.; Zhang, Y.; Lin, C.; Wang, X.; Dai, S. Improvement of Swanepoel method for deriving the thickness and the optical properties of chalcogenide thin films. *Opt. Express* **2017**, *25*, 440–451.
43. Okada, T.; Mugiraneza, J.; Shirai, K.; Suzuki, T.; Noguchi, T.; Matsushima, H.; Hashimoto, T.; Ogino, Y.; Sahota, E. Crystallization of Si Thin Film on Flexible Plastic Substrate by Blue MultiLaser Diode Annealing. *Jpn. J Appl. Phys.* **2012**, *51*, 03CA02.
44. Zhizhchenko, A.Y.; Tonkaev, P.; Gets, D.; Larin, A.; Zuev, D.; Starikov, S.; Pustovalov, E.V.; Zakharenko, A.M.; Kulinich, S.A.; Juodkazis, S.; others. Light-Emitting Nanophotonic Designs Enabled by Ultrafast Laser Processing of Halide Perovskites. *Small* **2020**, *16*, 2000410.

 doi:10.20944/preprints202010.0619.v1

Sample Availability: Samples are available from the authors.